Nuclear Instruments and Methods in Physics Research B 97 (1995) 402–406

ELSEVIER

NIM B
Beam Interactions with Materials & Atoms

Specular and off-specular anomalous X-ray scattering as quantitative structural probes of multilayers

H.E. Fischer [a,*], H. Fischer [b], O. Durand [c], O. Pellegrino [d], S. Andrieu [b], M. Piecuch [b], S. Lefebvre [a], M. Bessière [a]

[a] *LURE (CNRS / CEA / MESR), Bât. 209d, Univ. Paris-Sud, 91405 Orsay cedex, France*
[b] *Lab. Phys. Sol., Univ. Nancy I, B.P. 239, 54506 Vandoeuvre-lès-Nancy, France*
[c] *LCR Thomson-CSF, Domaine de Corbeville, 91404 Orsay cedex, France*
[d] *CECM, 15 rue Georges Urbain, 94407 Vitry-sur-Seine cedex, France*

Abstract

We have refined experimental techniques and developed theoretical analyses which allow a quantitative structural characterization of multilayers through X-ray diffraction. The use of both specular and off-specular measurements has provided probes of sample structure in the vertical (growth) direction and in the horizontal (parallel to interfaces) direction. In addition, by performing small-angle as well as large-angle diffraction measurements, both mesoscopic and atomic length scales are accessible. The advantages of high intensity and anomalous dispersion available with synchrotron radiation (LURE, Orsay) have greatly contributed to the quality of our data, for which the use of simulation programs has allowed a robust and precise extraction of several structural parameters, such as layer thicknesses, interfacial thicknesses, and interfacial correlation lengths. We have obtained results for a variety of samples, including several Fe/Ir and Mn/Ir superlattices (grown at different temperatures), three Fe/Pd superlattices (having controlled interface profiles), and a monolayer of SiO_2 grown on Si through dry oxidation. In this paper we present some representative results. The physical properties of such multilayer materials (e.g. magnetic and transport properties) are generally very dependent on their structural characteristics, in particular their interfacial structures.

1. Description of experiments

We will discuss results for two samples: 1) a very high quality Fe/Ir superlattice given by $(Ir_{25.7A}/Fe_{9.3A})_{45}/Ir_{140A}/MgO(001)$, and 2) a Mn/Ir superlattice given by $(Ir_{27A}/Mn_{15A})_{20}/Ir_{185A}$/sapphire, both produced at U. Nancy using molecular beam epitaxy (MBE) at $T = 100°C$. The samples were stored at room temperature and pressure since their growth approximately one year ago.

Our discussion will concentrate on the Fe/Ir sample. For this superlattice, the Ir layers are thick enough to assume their bulk fcc structure, while the relatively thin Fe layers are constrained to adopt a bct structure (c/a ratio of ~ 1.25) rather than the normal bcc structure. In-situ RHEED measurements indicated a nearly perfect monocrystalline growth.

The X-ray diffraction measurements were carried out using a 4-circle goniometer at the D23A anomalous dispersion beamline at the DCI synchrotron (LURE, Orsay). A Si(111) double-crystal sagittal-focusing monochromater gave sufficient energy resolution ($\Delta E/E \approx 10^{-4}$) to choose an X-ray energy only 10 eV below the LIII absorption edge of Ir (giving $\lambda = 1.1065$ Å). This choice allowed a attenuation of the intensity resulting from the thick Ir buffer layer, making the scattering from the superlattice more visible. The technique of anomalous dispersion was therefore a great advantage to the feasibility of these experiments, the inelastic scattering signal being impeded by a Ge(111) analyser crystal before the NaI detector.

2. Results and discussion

For structural characterization, X-ray diffraction has two principal advantages over other techniques (such as TEM): it is a non-destructive probe, and it measures structural parameters as averaged over the entire illuminated volume of the sample. We performed a variety of X-ray diffraction measurements both at small (SAXS) and large (LAXS) angles in order to probe both the mesoscopic and atomic structures, respectively. We will focus on our data for small angles.

* Corresponding author. Tel. +33 76207158, fax: +33 76483906, e-mail fischer@ill.fr.

SSDI 0168-583X(94)00363-7

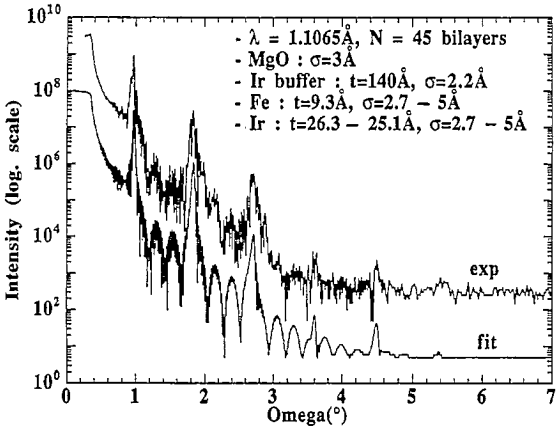

Fig. 1. Specular data (top) and simulation (bottom) for an ω–2θ scan (reflectivity curve) for the Fe/Ir superlattice, plotted as a function of the incident angle ω. The structural parameters determined from the simulations include the layer thicknesses t and the interface thicknesses σ. The two curves are separated for clarity.

Fig. 1 shows data and simulation results for the specular scattering (i.e. reflectivity) of the Fe/Ir sample at small angles, as a function of the incident angle ω. To perform these specular simulations, we employed the iterative formalism of Parratt [1] for calculating the X-ray reflectivity of a multilayer having rough interfaces, which is equivalent to matrix-method techniques such as that of Born and Wolf [2], both being full dynamical theories for specular scattering. The diffuse scattering contribution at the specular condition was first removed from the data by subtracting a shifted specular scan having $\omega = 2\theta/2 + 0.05°$. In addition to the layer thicknesses t, the figure legend also reports the fitted roughness amplitudes or interfacial thicknesses (quoted as standard deviations σ for the interface profiles).

We found that gradients (from the bottom to the top of the sample) in the Ir-layer thicknesses and in the interfacial thicknesses were necessary to simulate correctly the amplitudes of the superlattice peaks (appearing at angles of about 1°, 2° and 3° in the figure), especially those at higher orders. Such vertical thickness gradients occasionally occur during MBE growth, due to warmup effects. The more rounded oscillations in the diffraction pattern are due to the Ir buffer layer, and the high frequency oscillations are Kiessig fringes coming from the total thickness of the superlattice.

Since a perfect sample would not scatter any photons in a non-specular direction, we can obtain more direct information about structural imperfections by performing off-specular (i.e. diffuse-scattering) measurements. In addition, whereas specular X-ray scans probe the electron density of the superlattice in the vertical direction only (i.e. $\perp$ to the interfaces), off-specular scans also give structural informa-

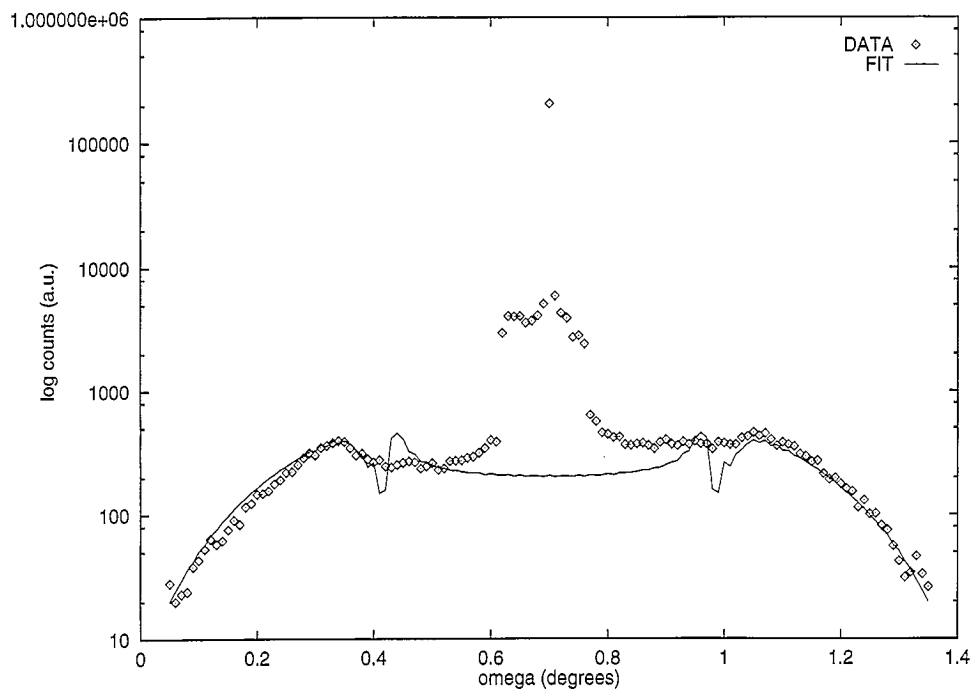

Fig. 2. Off-specular data (diamonds) and simulation (solid line) for an ω-rock about $2\theta = 1.4$ for the Fe/Ir superlattice, as a function of the incident angle ω. The simulation does not include the specular peak, whose base has been broadened due to the Lorentzian tails of the analyser crystal resolution function.

tion in the horizontal (x) direction, such as the horizontal correlation length ξ_x of the interfacial roughness [3].

We performed two types of off-specular scans for the Fe/Ir sample, both at small angles: i) ω-rocks (or rocking curves) having fixed 2θ, and ii) 2θ-rocks (or detector scans), having fixed ω. Our data and simulations for these two scans (about the same specular peak at $2\theta = 2\omega = 1.4°$) are shown in Fig. 2 (ω-rock) and Fig. 3 (2θ-rock). Note that the specular signal is not simulated, and that the apparent broadening at the foot of the specular peak is actually the interception of "analyser streaks" in the $q_x q_z$ reciprocal plane coming from the Lorentzian tails of the analyser crystal resolution function. An ω-rock at the first superlattice peak showed a specular FWHM of 0.005°, attesting to the extreme flatness of the sample's surface.

Fig. 2 clearly shows the presence of the Yoneda peaks, occurring when either the incident angle ω or the exit angle $\theta_{det} = 2\theta - \omega$ is equal to the critical angle of 0.35° for Ir at $\lambda = 1.1065$ Å (for a multilayer, it is sometimes possible to have a second critical angle coming from a lower interface). The simulation shows the specular + diffuse (dynamical effect) peak where ω and θ_{det} equal the angle for the first superlattice peak of Fig. 1 at $\sim 1°$. In the data, only the peak on the left is faintly discernable – the peaks may be washed out by a type of disorder in the sample which is not included in our model.

Fig. 3 carries considerable information – the single Yoneda peak is easily visible at the far left, followed by the specular peak (not simulated) at $\theta_{det} = 0.7°$ and then the "diffuse superlattice peaks" for orders 1, 2 and 3. These latter peaks are not resolution effects, but exist because the profiles of (possibly distant) neighboring interfaces are at least partially correlated in the growth direction. If adjacent interfaces were completely uncorrelated, the off-specular scattering in the right of Fig. 3 would have the form of a smooth monotonic decay to zero, without peaks.

To simulate these small-angle off-specular scans, we first employed the matrix-method technique of Vidal and Vincent [4] to calculate (dynamically) the specular electric fields at each interface of the sample, and then applied the theoretical results of Daillant and Bélorgey [5] for calculating the diffusely scattered intensity from these E-fields. Our approach leads to results similar to those of others [6], but with the advantage of incorporating the angular resolution of the detector explicitly in the calculation.

The two additional structural parameters that can be extracted from these off-specular scans are 1) the (average) horizontal correlation length ξ_x of the interfacial roughnesses (very approximately the distance between roughness "bumps" along an interface), and 2) the vertical correlation length ξ_z of the interfacial roughnesses (the distance in the growth direction over which the profiles of interfaces continue to track each other). All the other structural parameters of the off-specular simulations are exactly the same as those used in the specular simulation of Fig. 1.

The parameter ξ_x causes an amassing of diffuse inten-

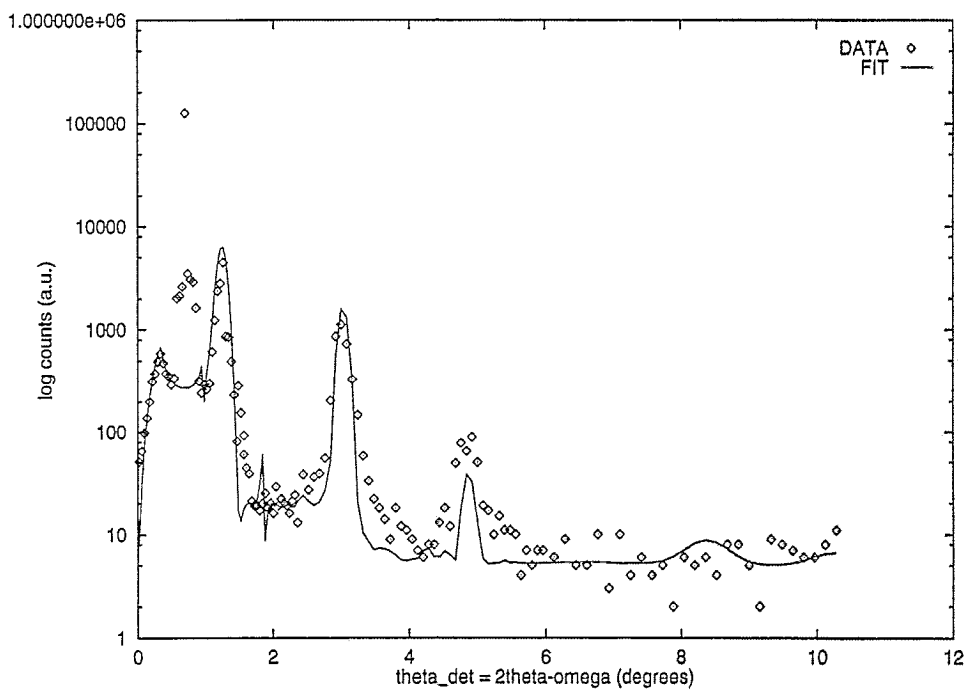

Fig. 3. Off-specular data (diamonds) and simulation (solid line) for an 2θ-rock about $\omega = 0.7$ for the Fe/Ir superlattice, as a function of the detector angle $\theta_{det} = 2\theta - \omega$. The specular peak is hence the same as that in Fig. 2.

sity in the q_x direction around the specular ridge (where q_x lies in the scattering plane and is parallel to the sample's surface), while ξ_z causes an amassing of diffuse intensity in the q_z direction around all specular peaks (including Kiessig fringes). In both cases, the parameters can be estimated as 2π/(FWHM in $q_{x,z}$ of diffuse intensity). Our simulations correctly incorporate the effects of ξ_x, but to treat ξ_z properly would require a full dynamical theory for diffuse scattering, instead of the dynamical-specular/kinematic-diffuse theory which we are using.

Nevertheless, since the angles of our superlattice peaks are all sufficiently larger than the critical angle, a kinematic treatment of diffuse scattering suffices for simulating the widths of the diffuse superlattice peaks in q_z (i.e. the off-specular peaks given by the amassing of diffuse intensity in q_z around specular superlattice peaks), once ξ_z has been incorporated into an appropriate interface correlation function. For $z_a(x)$ and $z_b(x)$ being the vertical displacements (about average altitudes of $z_{0,a}$ and $z_{0,b}$) of two interfaces in the sample along the x direction, we defined our interface correlation function as:

$$\langle z_a(x) z_b(0) \rangle = \sigma_{z,a}\sigma_{z,b}\ \mathrm{e}^{-x^2/\xi_x^2}\ \mathrm{e}^{-(\Delta z)^2/\xi_z^2}$$

where $(\Delta_z)^2 = (z_{0,a} - z_{0,b})^2$, and implying a Hausdorf dimension of 2 ($h = 1$) for the interfaces (i.e. Gaussian roughness).

Since our Fe/Ir sample turned out to have a rather small ξ_x, it was not possible to determine this ξ_x through the FWHM of the diffuse scattering in an ω-rock at small angles, since the rocking curve was not broad enough [7]. However, the total diffuse scattering is also directly proportional to ξ_x, allowing this parameter to be extracted after the diffuse signal is properly normalized – note that this proportionality implies that a sample having perfectly interdiffused interfaces (i.e. $\xi_x = 0$, which in reality is always limited by atomic size) would produce no off-specular signal even for large σ. The parameter ξ_x serves to distinguish interfacial roughness ($\xi_x \gtrsim 15$ Å) from interfacial diffusion ($\xi_x \lesssim 15$ Å).

By normalizing the ω-rock data of Fig. 2 with respect to the plateau of total specular reflectivity below the critical angle, we were able to extract a value of $\xi_x = 30$ Å. However, uncertainties in the angular dispersion of the incident beam, as well as the exact "footprint" correction for the reflectivity plateau, limit the precision of this result to a range of about 20 Å $< \xi_x <$ 50 Å. The angular resolution width of the analyzer crystal, nevertheless, was measured and incorporated in the calculations (as a Gaussian resolution function).

Since a 2θ-rock carried out to large detector angles accumulates an appreciable q_x component, the effects of ξ_x can also be seen in the data of Fig. 3. A value of ξ_x larger than about 100 Å steepens significantly the overall decreasing intensity to the right of the specular peak. We found that a value of $\xi_x = 30$ Å was consistent with that needed to prop up the 3rd diffuse superlattice peak at $\theta_{\mathrm{det}} \sim 5°$. We intend to continue to refine our simulation results, but the large computation time (several hours for one off-specular diffraction pattern) makes the iterations rather slow.

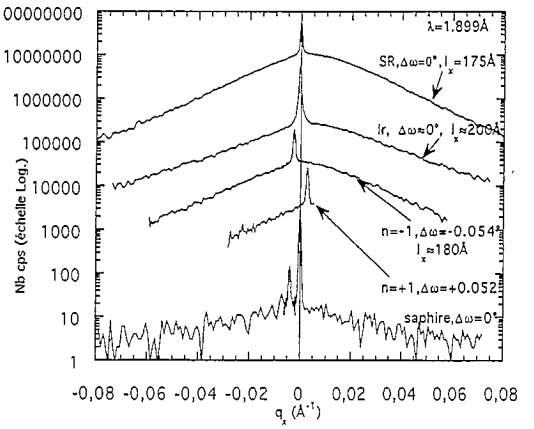

Fig. 4. Off-specular large-angle data for ω-rocks around several peaks in the vicinity of the first order atomic Bragg peak of the Mn/Ir superlattice, plotted as a function of the transverse momentum change q_x.

Since ξ_x was determined (approximately) from beam normalization factors, and the other structural parameters where taken from the specular simulations, the only free parameter for the off-specular fits was ξ_z. We found that to match the q_z widths of the diffuse superlattice peaks in Fig. 3, as well as to suppress the amplitudes of the high-frequency diffuse Kiessig fringes, we needed a value of $\xi_z \sim 200$ Å. As expected, ξ_z had a very small effect on the ω-rock simulation, since ω-rocks are almost exactly along the q_x direction.

We also performed ω-rocks at large angles for the Mn/Ir superlattice, shown in Fig. 4. The peak "SR" corresponds to the first order atomic Bragg peak for the average vertical plane spacing of the superlattice (i.e. $N = 0$). Also shown are the satellite peaks at $N = 1$ and $N = -1$, the Ir buffer peak ("Ir"), and finally the substrate "saphire" peak (which shows multiple peaks in q_x, possible due to atomic steps at the interface). Specular peaks are visible above the broader diffuse scattering peaks. Although we have not yet developed satisfactory simulations for these off-specular large-angle data, one can identify a horizontal correlation length l_x for atomic disorder as being inversely proportional to the q_x widths of the Gaussian-like diffuse scattering peaks. The l_x values reported in the figure were extracted as $l_x = 2\pi$/FWHM. The off-centering of the $N = 1$ and $N = -1$ peaks is due to a miscut angle in the substrate, producing the same angle in reciprocal space between the satellite peaks and the atomic Bragg peaks.

3. Conclusions

Using a single set of structural parameter values, we have simulated specular and off-specular diffraction patterns at small angles for a high quality Fe/Ir superlattice (Figs. 1, 2 and 3). We find that our dynamical-specular/kinematic-diffuse scattering model succeeds reasonably well in simulating the off-specular data, and allows an approximate, but quantitative, extraction of the interfacial correlation lengths ξ_x and ξ_z, which are not accessible from specular data. We have also shown that complimentary information about structural disorder (on atomic length scales) can be obtained through analysis of high-angle off-specular data (Fig. 4). Fruitful discussions with J. Daillant are appreciated.

References

[1] L.G. Parratt, Phys. Rev. 95 (1954) 359.
[2] M. Born and E. Wolf, Principles of Optics, 6th corr. ed. (Pergamon, Oxford, 1980) p. 55ff.
[3] S.K. Sinha et al., Phys. Rev. B 38 (1988) 2297.
[4] B. Vidal and P. Vincent, Appl. Opt. 23 (1984) 1794.
[5] J. Daillant and O. Bélorgey, J. Chem. Phys. 97 (1992) 5284.
[6] V. Holý and T. Baumbach, Phys. Rev. B 49 (1994) 10668.
[7] We have, however, successfully extracted ξ_x values from the FWHM of ω-rocks at higher q_z values (but still at small angles) for several Fe/Cr superlattice samples.